Selective laser powder bed fusion for manufacturing of 3D metal-ceramic multi-materials assemblies

Frédéric Veron, Fabien Lanoue, Valérie Baco-Carles, Kateryna Kiryukhina, Olivier Vendier, Philippe Tailhades

Selective laser powder bed fusion for manufacturing of 3D metal-ceramic multi-materials assemblies

Frédéric Veron[1-2], Fabien Lanoue[1], Valérie Baco-Carles[2],
Kateryna Kiryukhina[1], Olivier Vendier[3], Philippe Tailhades[2]

1- Centre National d'Etudes Spatiales CNES, 18 Avenue Edouard Belin, 31 400 Toulouse, France
2- Institut Carnot Chimie Balard Cirimat, UMR CNRS 5085 Cirimat, Université Paul Sabatier, 118 Route de Narbonne, 31 062 Toulouse, France
3- Thales Alenia Space, 26 Avenue Jean François Champollion, 31 100 Toulouse, France.

Abstract: The technology of laser fusion on a powder bed is modified for the manufacture in air, of multi-material parts formed in the three dimensions of space, with zones which can be either a dielectric ceramic, based on alumina, or an aluminum - silicon metallic conductor. This additive manufacturing method uses only one powder. This powder is an AlSi12 alloy previously activated by a chemical treatment, which gives it, increased reactivity to oxygen. Therefore, the only adjustment of the manufacturing conditions, through the power and the scanning speed of the laser, as well as the hatch spacing, makes it possible to choose the construction of ceramic or metallic type zones. The modification of AlSi12 powders by chemical activation is the subject of a detailed characterization, allowing the selection of treatment conditions adapted to the multi-material manufacturing process. The ceramic or metallic areas that are produced, are also characterized for subsequent use of this process, for the manufacturing of microwave devices dedicated to the space industry.

Keywords: Laser powder bed fusion, AlSi12, 3D multimaterials, metal ceramic assemblies, selective laser oxidation, microwave devices

1. Introduction

A few additive manufacturing techniques allow the production of parts combining in space and in a controlled manner, different materials. Among the seven families of currently standardized processes [1][2], this is particularly the case for inkjet printing (3D printing), wire fusion (material extrusion) and to a lesser extent powder projection in a laser energy flow (Direct Energy Deposition). The laser fusion on a powder bed, on the other hand, is ill-suited to the direct production of parts or assemblies comprising distinct parts, made of different materials. This is a limitation, which prohibits the use of this manufacturing process for certain technological applications. When it comes to building in a single step, parts of complex shapes requiring the combination of a metal conductor with a dielectric, there is no solution to this day using only this single process. Such associations in parts of complex shapes would however be very advantageous for constituting for instance, microwave components of reduced size. The introduction of a ceramic which dielectric constant would be close to ten, in today's conventional waveguides, would indeed allow a reduction in their size by a factor close to three, according to the work of Paknys [3]. There is therefore a real challenge to be taken up in order to increase the possibilities of this additive manufacturing technology, which is

already well established in various economic sectors, particularly in the aeronautics and space sector.

In this work, we tried to solve this problem by looking for a way allowing both to fuse a metallic powder, to form electrically conductive zones, and to oxide and sinter the initial powder, to create dielectric zones. The choice of the powder was oriented towards the eutectic alloy AlSi12 melting from 577°C and very frequently used for additive manufacturing by laser fusion [4][5][6][7] or for molding [8]. Beyond the industrial availability of this alloy in the form of powders suitable for additive manufacturing and numerous bibliographic data on its use in Selective Laser Sintering / Selective Laser Melting machines [9][10][11], the AlSi12 alloy presents the advantage of being able to be fused in air in the metallic state. However, AlSi12 alloy is mostly aluminum, although it contains small precipitates of metallic silicon [12]. Since aluminum is located very low in the Ellingham-Richardson diagram [13], suitable processing and manufacturing conditions, leading to its oxidation and then its sintering, are therefore potentially possible.

In fact, the highly oxidizable nature of aluminum, which can be used for instance in solid propellants [14][15] or nano-energetic materials for MEMS [16], means that it cannot be encountered in Nature in the metallic state and that it is not possible to stabilize it in air without it being coated with an oxide-type layer, most often alumina [17][18][19]. This very dense layer, which is not very permeable to oxygen, is generally very protective. It thus makes it possible to handle aluminum alloy powders in air [20][21]. Aluminum alloy powders can thus, without particular difficulty, be fused by a laser beam in the metallic state, the alumina only appearing in very small quantities at the surface or at the grain boundaries. However, any damage to the passivation layer very quickly generates oxide formation in the affected region, given the natural propensity of aluminum to oxidize.

It therefore seemed interesting to us to try to take advantage of this dichotomy, passivation and oxidability, to manufacture by laser fusion on a powder bed, parts comprising metal and ceramic regions. Preliminary tests, however, failed to properly oxidize and sinter the AlSi12 base alloy, despite high-power laser beam irradiation or relatively prolonged exposure to the focused light energy source.

The basic idea that was followed was therefore to weaken the protective character of the thin oxidized layer, enveloping the grains of AlSi12 alloy, in order to increase their reactivity with respect to oxygen. Depending on the setting of the laser beam (power, scanning speed, hatch spacing, etc…), it should then be possible either to melt and merge these grains in the metallic state, or to oxidize and sinter them, to form the electrically conductive metal areas on the one hand, and the oxide type areas having a dielectric character, on the other hand.

Aluminum, even protected by a thin oxide layer, can easily be etched by alkali hydroxides [22][23] to form aluminates or hydroxides. To weaken the protective character of the alumina layer located on the surface of AlSi12 alloy grains, simple chemical etching by an alkali hydroxide was therefore an interesting route, capable of leading to powders, which can be fused to metallic state or oxidized and sintered as oxide, by a laser beam.

This paper is therefore divided into two main parts. The first studies the effects of chemical etching of an AlSi12 alloy powder, by different concentrations of sodium hydroxide solutions. The objective here is to transform the thin protective layer coating the alloy grains, in order to make it less protective against oxidation and to obtain an AlSi12 powder, which will be qualified as "activated". An activated AlSi12 alloy powder is, in the second part of the paper, processed in a laser fusion additive manufacturing machine. Thanks to the appropriate adjustment of the manufacturing conditions, parts combining metallic conductive areas and dielectric ceramic-type areas, are produced for the first time by a laser process. The samples are characterized at the structural and microstructural level.

2. Materials and Methods

2.1. *Samples*

An AlSi12 powder PS2585-18 from 3D System was used for the experiments. This consists of spherical grains, the median grain size of which is close to 25 micrometers. The grains contain two metallic phases, aluminum and silicon, as revealed by X-ray diffraction. The alloy powder was treated with sodium hydroxide solutions of different concentrations from 0.03 to 10 $mol.L^{-1}$. For this chemical treatment, one gram of powder was mixed with one cubic centimeter of sodium hydroxide solution. The resulting samples were then dried at about 100°C to remove the excess of water. They were then the subject of various characterizations making it possible to understand the modifications undergone by the initial alloy powder. These characterizations also made it possible to select an etching process with a view to additive manufacturing experiments intended for the production of parts comprising metallic or ceramic type zones.

2.2. *Additive manufacturing machine*

A 3D Systems ProX200 type laser fusion machine on a powder bed was implemented. The laser beam emitted by this machine has a wavelength of 1070 nm. It is focused in the form of a gaussian spot of 75 micrometers, on a work plate of 140 x 140 mm^2. Its power can be regulated between 30 and 300W by step of 3W.

2.3. *Analytical techniques*

The crystalline structure of the samples was studied using Bruker AXS D4 Endeavor diffractometer equipped with a 1D LynxEye detector. Kα radiations ($\lambda K\alpha_1$= 0.15405 nm and ($\lambda K\alpha_2$= 0.15443 nm) emitted by a copper anode, were used as X-ray source. The Kβ ray was eliminated by a nickel filter. A second diffractometer (Bruker Advance D8) equipped with a heating set-up, was used to study the samples in the temperature range from room temperature up to 1 100°C. The same wavelength was used. The chemical bonds were also characterized by Fourier transform Infrared spectroscopy using a Nicolet 6700 of Thermofisher Scientific, in the spectral range lying from 400 to 4 000 cm^{-1}.

The microstructure of the samples and the patterns written by the laser, were observed by optical (Optical numerical microscope VHX 1000 from Keyence) and scanning electron (Jeol JSM 6510LV) microscopes. Their chemical composition was analyzed by Energy

Dispersive Spectrometry (EDS) with a Brucker Quantax electron microscope analyser. The metallic powders were pressed under 750 MPa to make green compacts. A focused ion beam combined with field effect emission gun (SEM/FIB FEI Helios 600i) associated with Oxford Instruments AZTEC Advanced electron microscope analyser, were used to prepare cross-sections for chemical and microstructural characterizations.

The optical properties of the powders of AlSi12 alloy, before and after chemical treatment, were analysed by a Bentham PVE 300 photovoltaic characterization system, with integrating operation mode. Their specific surface area was measured by a Tristar 3020 of Micromeritics, using the Brunauer, Emmett and Teller model (BET). The adsorbed gas was nitrogen. The thermal behavior of the AlSi12 powders was studied by thermogravimetric analysis using a Setaram TAG 16. The powder was degassing under primary vacuum at 50°C for 12 hours. Apparent densities of activated AlSi12 alloys powders were characterized by Electrolab EV-O2 volumeter. Surface roughness analyses were carried out with Sensofar S-NEOX focused variation microscope. Dielectric properties of ceramic areas were analyzed by a Keysight N5247B PNA-X microwave network analyzer.

3. Results and discussion

3.1 Effect of the sodium hydroxide solutions on AlSi12 powder

After treatment by sodium hydroxide of the AlSi12 alloy powder, the X-ray diffractograms (Fig. 1) show that the intensity of the diffraction peaks ascribed to aluminum decreases appreciably, unlike that of the silicon peaks, which remains approximately constant. This observation suggests that the secondary phases resulting from chemical etching are formed essentially from the aluminum oxidation released by dissolution of the metal. It is in fact observed that the new phases formed, identified by X-ray diffraction, contain high contents of this element. For sodium hydroxide concentrations lying from 1 to 3.34 mol.L^{-1}, it is aluminum hydroxide which appears. At higher content (10 mol.L^{-1}), a sodium aluminosilicate is detected.

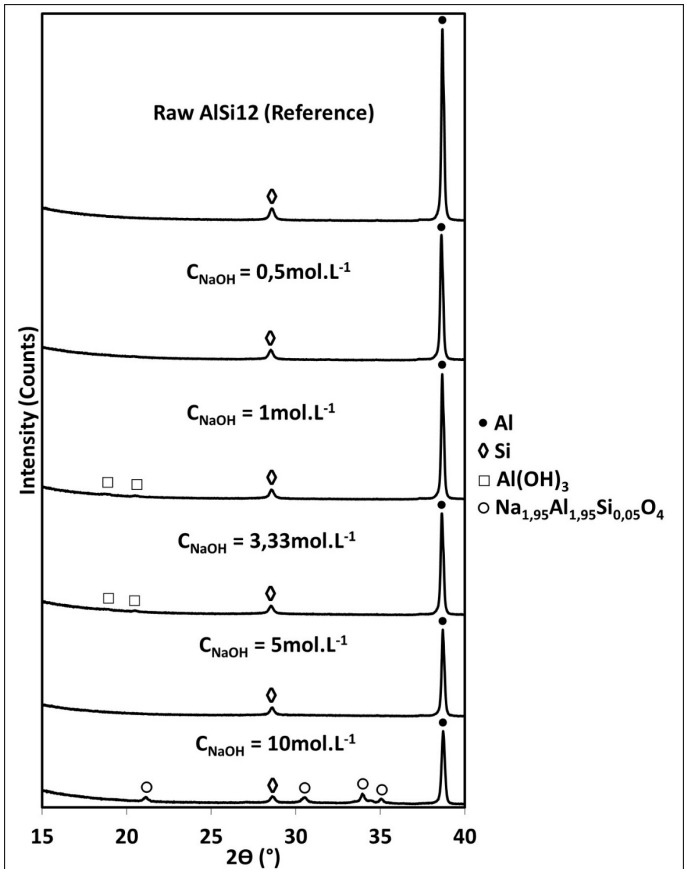

Figure 1: X-ray diffraction patterns of sodium hydroxide pre-treated AlSi12 powders with different concentrated solutions and AlSi12 reference.

Infrared spectroscopy (Fig. 2) reveals however, that other additional compounds appear, probably at very low levels or in poorly crystallized forms, so that their detection escapes X-ray diffraction. However, the identification of these compounds is not easy, even by infrared spectroscopy. The interpretation that is given is based on the comparison of the spectra of the treated powders with the spectra of reference substances, but also on the observation of EDS maps obtained for characteristic samples (see subsequent comments on figure 4).

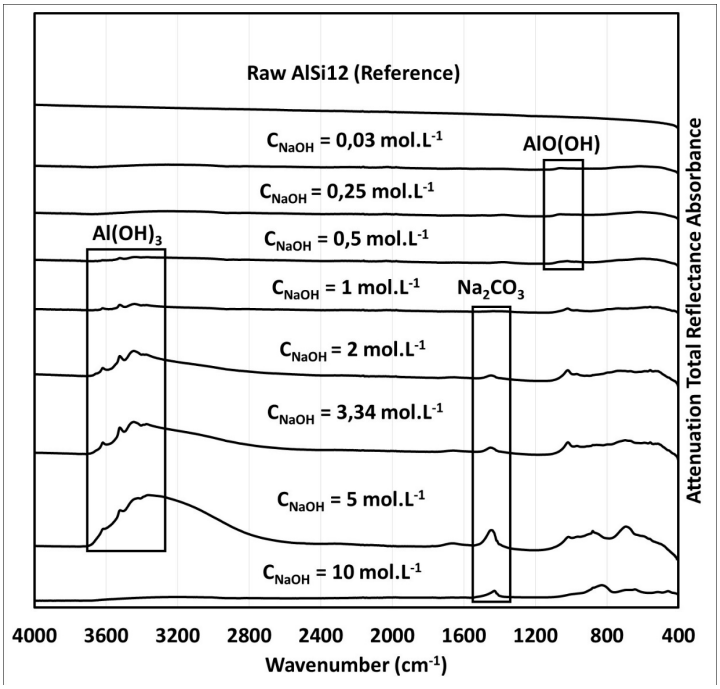

Figure 2: Infrared spectra of sodium hydroxide pre-treated AlSi12 powders with different concentrated solutions and AlSi12 reference.

Chemical treatment carried out with solutions of low concentrations (≤ 0.5 mol.L^{-1}) generates aluminum oxyhydroxide, some broad characteristic bands of which can be detected on the infrared spectra of the samples studied (Fig. 3). For the sample treated with a 0.5 mol.L^{-1} solution however, this oxyhydroxide seems to coexist with aluminum hydroxide. EDS maps also confirm the coexistence of aluminum and oxygen at the aluminum-silicon grain surface (Fig. 4). This observation is consistent with the formation of hydroxide or oxyhydroxide phases at the periphery of the grains. Associated with these phases, the maps also reveal the presence of sodium and carbon elements, which are constitutive of the carbonate Na_2CO_3 observed on the IR spectra of the samples treated with concentrated solutions (≥ 1 mol. L^{-1}, Figure 2).

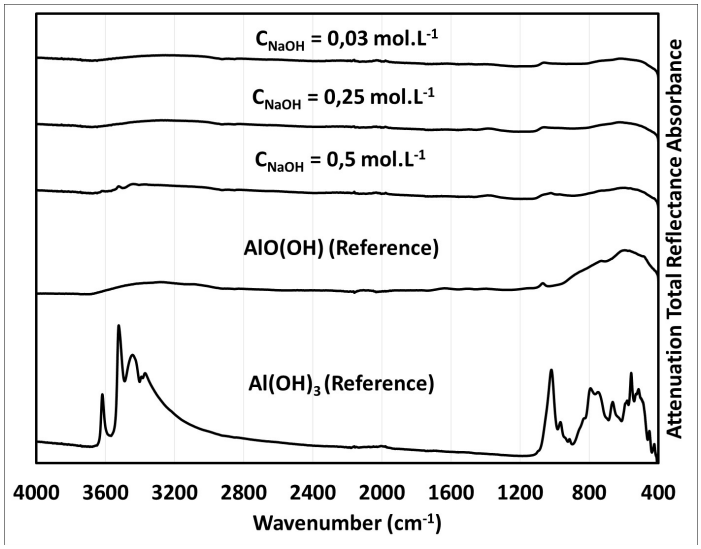

Figure 3: Infrared spectra of sodium hydroxide pre-treated AlSi12 powders with the most diluted solutions and material references.

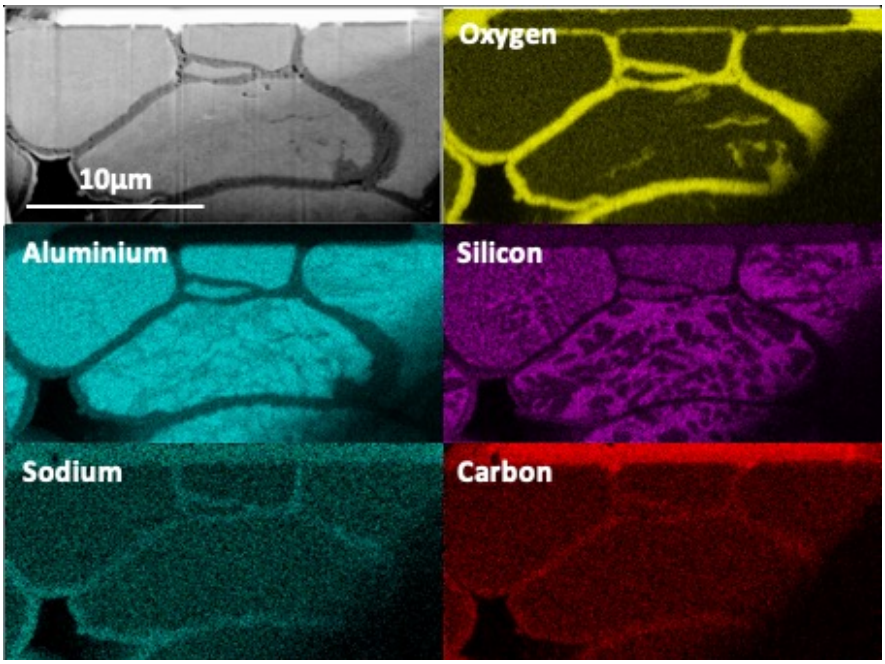

Figure 4: Scanning electron micrograph and related EDS mapping of FIB cross-section of sodium hydroxide pre-treated (C_{NaOH}=0.25mol.L^{-1}) AlSi12 compacted powder grains.

The chemical reactions involved could be, as Godart [24] showed, an etching on the metal by the water for the low concentrated basic solutions, according to equations:

$2Al + 6H_2O \rightarrow 2Al(OH)_3 + 3H_2$ for T < 21°C (1)

$2Al + 4H_2O \rightarrow 2AlO(OH) + 3H_2$ for 21°C < T< 100°C (2)

The treatments of the powder were in fact carried out at room temperature, the sodium hydroxide mixture with AlSi12 having been dried at 100°C.

The previous EDS maps also reveal, on the surface of the grains, a region containing both sodium and carbon. Sodium carbonate is then suspected, knowing that the carbonate ions dissolved in the hydroxide solution can generate the reaction [25]:

$CO_2 + 2NaOH + H_2O \rightarrow Na_2CO_3 + 2H_2O$ (3)

The formation of carbonate is also confirmed by infrared spectroscopy (Fig. 2 and 5) for powders treated with more concentrated solutions (1 to 10 mol.L^{-1}). Aluminum hydroxide is also clearly present in these samples. According to the work of Bolt [26], the phases obtained would result from the succession of the following two global reactions:

$2Al + 6H_2O + 2NaOH \rightarrow 2NaAl(OH)_4 + 3H_2$ (4)

$2NaAl(OH)_4 + CO_2 + H_2O \rightarrow 2Al(OH)_3 + Na_2CO_3 + 2H_2O$ (5)

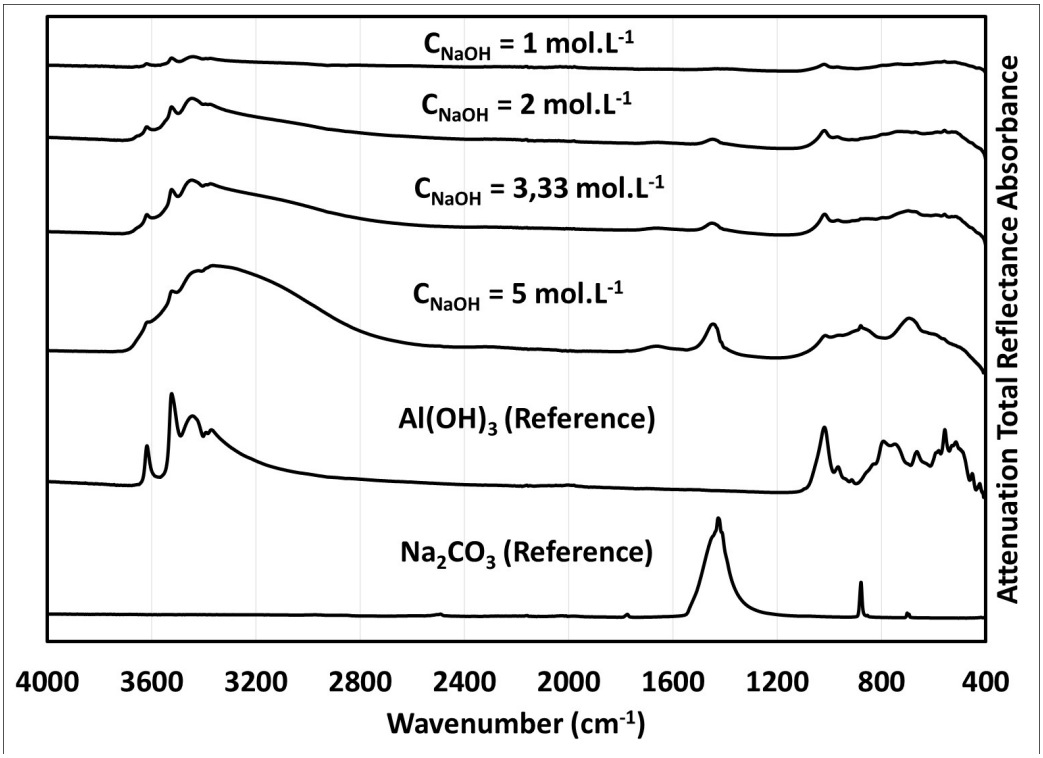

Figure 5: Infrared spectra of sodium hydroxide pre-treated AlSi12 powders with moderate concentrated solutions and material references.

The chemical etching proceeds from the surface towards the core of the grains. Figure 4 gives an illustration for a sodium hydroxide concentration of 0.25 mol.L^{-1}. However, figure 6 gives a more complete view, showing in particular that the very fine and dense oxide layer, present on the surface of the initial grains of AlSi12, is considerably modified by the chemical treatments. A relatively porous layer, the thickness of which increases as a function of the concentration of the sodium hydroxide solution, replaces it. For the highest concentrations, the grains are not only etched on the surface, but also in their core, where only a few small nuclei of metallic nature remain.

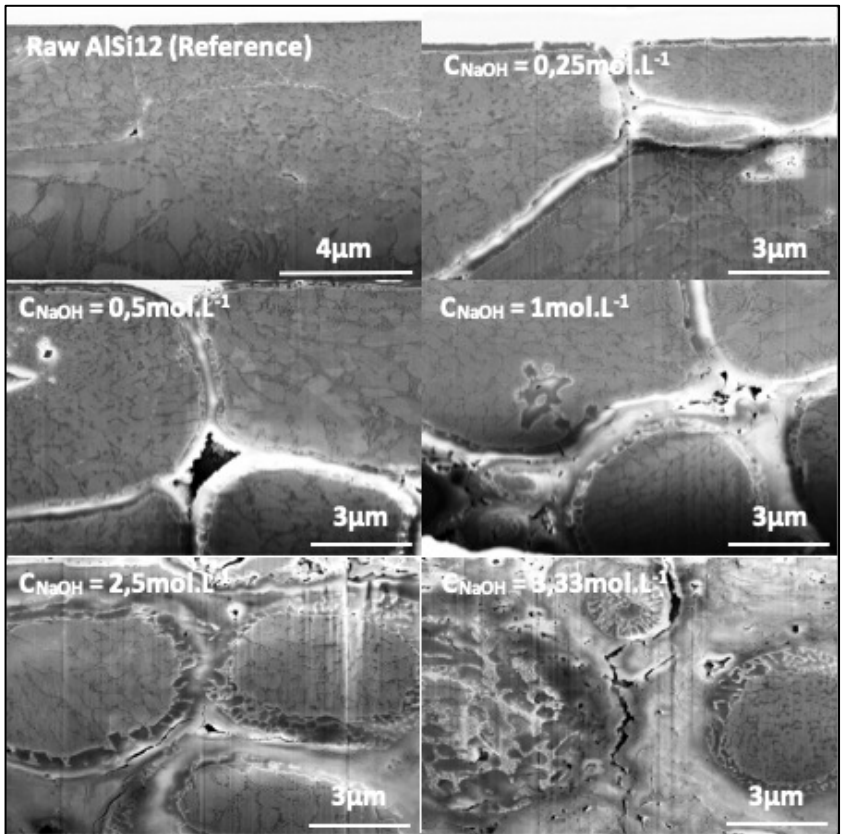

Figure 6: Scanning electron micrographs of sodium hydroxide pre-treated AlSi12 compacted grains with different concentrated solutions and AlSi12 reference.

The surface layer created by chemical treatment has a strong impact on the optical properties of the powder. The absorbance of the initial powder at the wavelength of the laser (1070 nm) of the additive manufacturing machine used subsequently, thus suddenly increases from 0.65 to more than 0.8, even after the etching by the least concentrated sodium hydroxide solution (0.03 mol.L^{-1}). At such a concentration, the thickness of the surface layer is only 300nm. Significant changes are also seen in the specific surface area of the powder, which is large when aluminum oxyhydroxide predominates (Fig. 7). This suggests that the oxyhydroxide formed is very porous and from this point of view, extremely different from the passivation layer of the initial alloy. Finally, the apparent density of the powder decreases significantly when the powder is more strongly etched (Fig. 7). The development of porosities and the surface roughness of the grains, which hinders spontaneous compaction, are at the origin of this evolution.

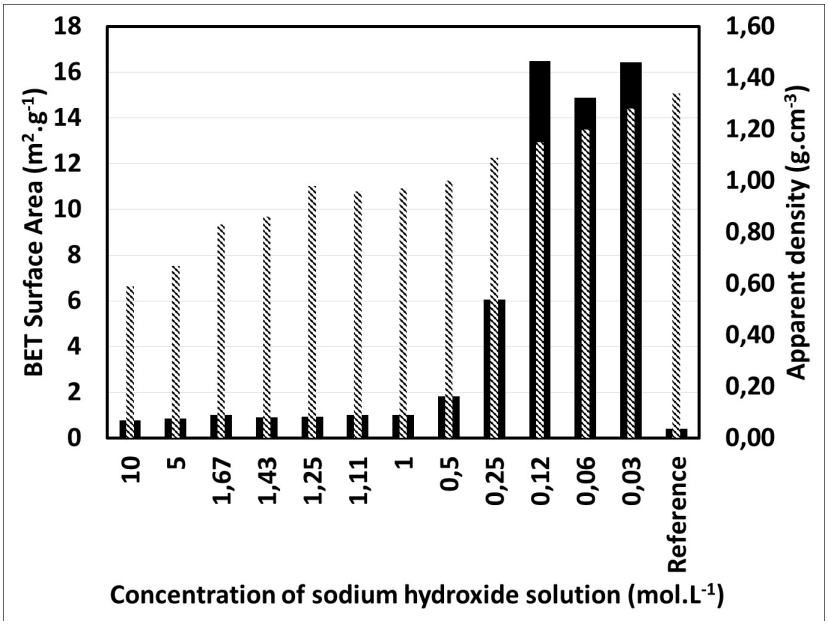

Figure 7: Specific surface areas (filled bars) and apparent densities (striped bars) of sodium hydroxide pre-treated AlSi12 powders with different concentrated solutions.

Selection of AlSi12 powders treated by sodium hydroxide

The final objective of the present work is to manufacture by laser fusion on a powder bed, parts made up of conductive metal regions, on the one hand, and ceramic-type dielectrics, on the other. The preceding treatments with sodium hydroxide are certainly intended to increase the reactivity of the alloy powders, but they must also retain their predominantly metallic nature. After melting, these powders must in fact form the conductive metal zones. A first selection of the activated powders was therefore made by testing their ability to conduct electricity after a simple compacting.

For this, the powders were pressed at 750 MPa in a stainless steel die, in order to form, after demolding, discs 5 mm in diameter and 5 mm in thickness. The ability of the disks to conduct electricity was evaluated by an ohm-meter connected to their two opposite surfaces. Although this test is approximate, it is very discriminating. It makes it possible to show that for chemical treatments employing concentrations greater than, or equal to 3.3 mol.L^{-1}, the compacts no longer conduct electricity. Consequently, the powders thus treated cannot be selected for the additive manufacturing of multi-material parts.

This first selection made, the reactivity of the remaining powders was evaluated from thermogravimetric analyzes. Admittedly, the heating conditions in a thermo-balance are very different from those resulting from irradiation by a laser beam, but thermogravimetry nevertheless makes it possible to reveal the aptitude of a powder to be oxidized. It also makes it possible to make useful comparisons for a second level of selection.

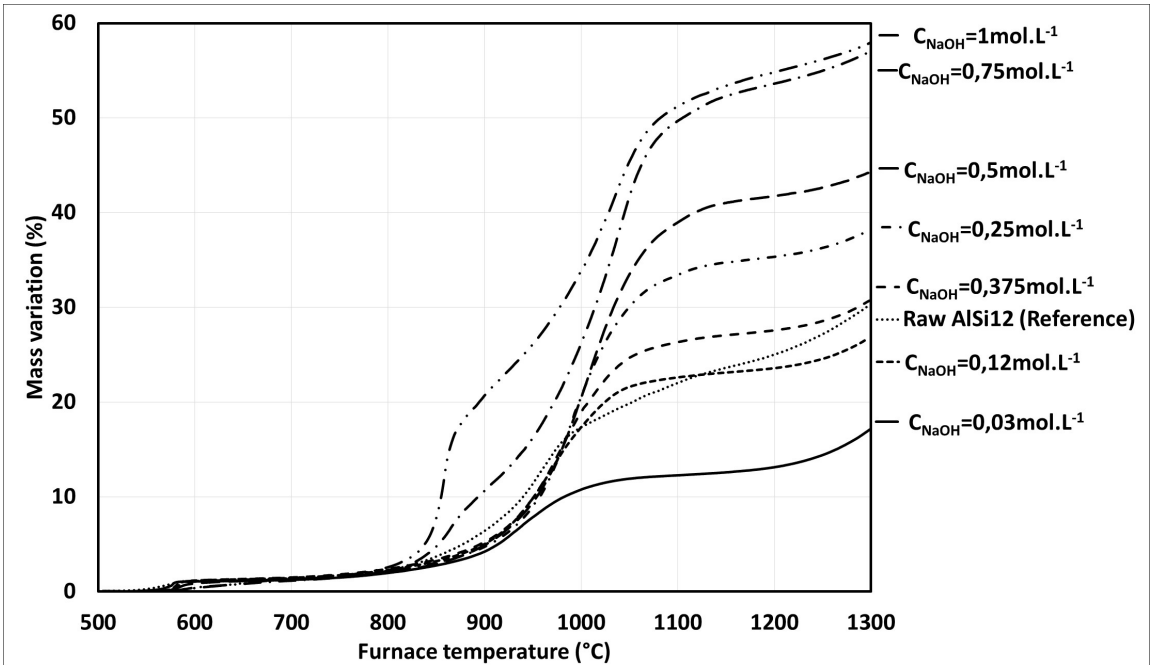

Figure 8: Thermogravimetric analyses of sodium hydroxide pre-treated AlSi12 powders with different concentrated solutions and AlSi12 reference. Heating rate is 2.5°C.min^{-1} under air atmosphere with prior vacuum degassing at 50°C during 12h.

Analyzes were therefore carried out on the powders treated with sodium hydroxide concentrations less than or equal to 1 mol.L^{-1}. These analyzes demonstrate a first gain in mass, which occurs in the vicinity of the melting temperature of the AlSi12 alloy (577 ° C) for all the powders studied. The melting of the metal, reflected by the disappearance of the diffraction peaks of the metal alloy (Fig. 9), indeed facilitates a slight oxidation. The latter, however, only very weakly increases the diffraction peaks attributed to the oxide γ-Al_2O_3 (Fig. 9).

Since the aluminum has been preferably oxidized by the sodium hydroxide treatments, the initial eutectic alloy is all the more depleted in this element as the hydroxide concentration is high. The remaining alloy therefore has a higher melting point. This is the reason why the oxidation in air at about 600°C, revealed by thermogravimetry, shifts towards high temperatures for powders treated with the highest sodium hydroxide contents.

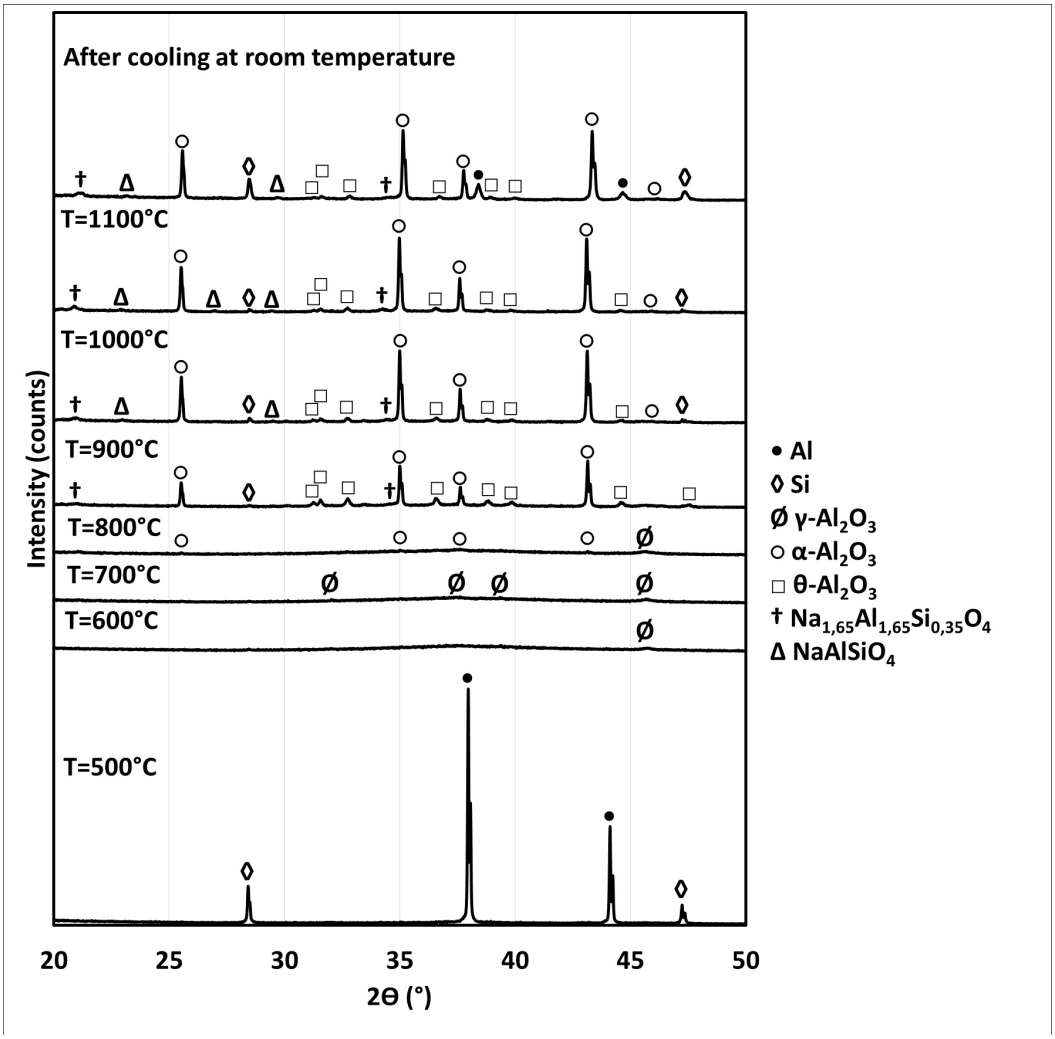

Figure 9: X-ray diffraction patterns obtained by *in-situ* heating at different temperatures of sodium hydroxide pre-treated AlSi12 powder with 1 mol.L^{-1} solution.

At temperatures above about 800 °C, oxidation accelerates and essentially reveals the alpha and theta allotropic varieties of alumina. X-ray temperature diffraction also reveals a peak, which could be attributed to $NaAlSiO_4$ (Fig. 9). These oxidations occur at lower temperatures for powders treated with high concentrations. Their reactivity towards oxygen is clearly increased compared to the initial alloy powder. On the other hand, for concentrations below 0.25 mol.L^{-1}, the chemical treatment does not increase the reactivity. It would even seem that it tends rather to passivate the powders, at least for the lowest concentrations and at the lowest temperatures.

3.2. Powder bed fusion with "activated" powders of AlSi12 – Manufacture of parts made of metallic and dielectric zones

All of these results therefore lead to consider only the powders treated by sodium hydroxide concentrations between 0.25 and 1 mol.L^{-1}, for the manufacture of metal-oxide multi-material in laser fusion on a powder bed. Considering that the major difficulty lied in the oxidation of the AlSi12 powder under a laser beam, it seemed relevant to initiate manufacturing tests with the powder whose reactivity was the most strongly enhanced,

namely the powder treated by a 1 mol.L^{-1} solution. For this reason, the following additive manufacturing experiments were carried out with such a powder.

Laser fusion on a powder bed offers a very large number of parameters likely to influence the production of parts with a given material (laser power, scanning speed, hatch spacing, powder bed thickness, compaction rate, atmosphere, laser focusing, ...). It is in practice impossible to explore all the combinations of these parameters. This is the reason why we have set some of them at values deemed reasonable and suitable for the production of the multi-material ceramic-metal parts targeted. The ambient air was thus chosen the manufacturing chamber atmosphere (# 20% oxygen and 80% nitrogen). Since parts based on AlSi12 alloy can be manufactured in air, one could indeed hope to manufacture metal in this atmosphere, even with an alloy pre-treated with sodium hydroxide. Moreover, the oxygen in air was also essential for the oxidation of the metal necessary to make the ceramic regions. The thickness of the powder bed was set at 50 micrometers, taking into account in particular, the particle size of the AlSi12 powder used (see experimental part). The laser spot size was focused on the surface of the powder bed. Its diameter was close to 75 micrometers. An hexagonal pavement was chosen to build the parts (diameter in which the hexagon is inscribed equal to 10 mm). On the other hand, the good combinations of power, speed of movement of the laser and hatch spacing leading to coherent parts, at the same time dense and not very rough, have been sought, not only to form the metallic zones, but also to obtain the ceramic zones. Such experiments were led on cubic parts of 1 x 1 x 1 cm^3.

3.3 *Metallic areas*

For metallic areas, the ranges explored were 30 to 270 W for power, 100 and 1 800 mm.s^{-1} for scanning speed and 10 to 180 μm for hatch spacing. For the lowest powers (<40 W), the melting of the metal grains is not done correctly. These remain in powder form and the parts cannot be constructed. At high powers (i.e. higher than about 60 W), the laser shock tends to expel the metal powder from the irradiated areas, in particular when the scanning speed is high (> 400 mm.s^{-1}). So, parts cannot be built either. Deformed parts made of large metal aggregates are best obtained for scanning speeds of between 100 and 400 mm.s^{-1}. However, for a scanning speed of 100 mm.s^{-1}, there is a fairly wide range of power (approx. 50 to 70 W) and hatch spacing (approx. 20 to 180 μm), in which parts with a very high good mechanical cohesion, regular geometry and relatively smooth surface can be produced (Fig. 10).

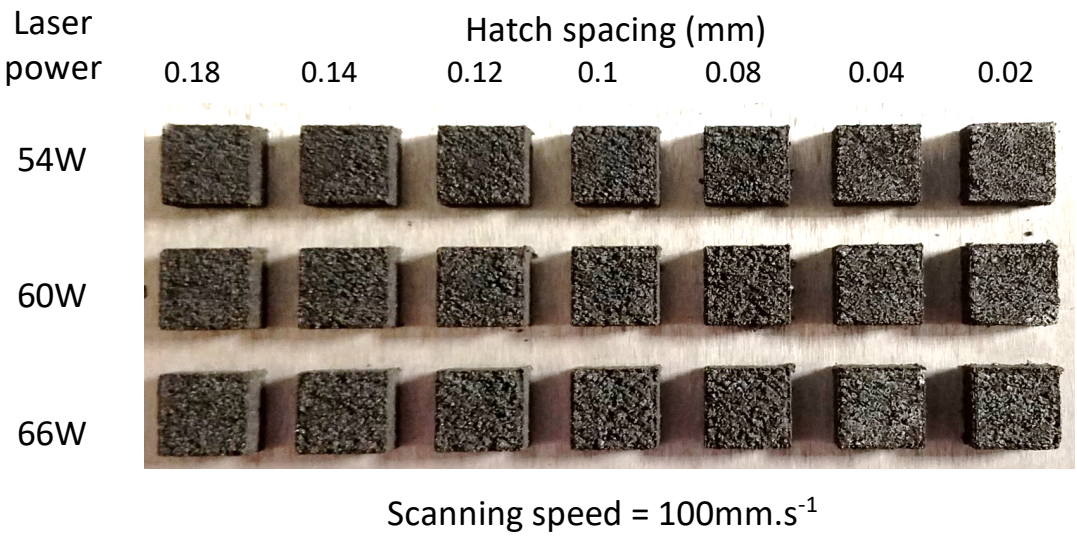

Figure 10: Conductive samples manufactured from sodium hydroxide pre-treated AlSi12 powder with 1mol.L^{-1} concentrated solution. Parameters (laser power, scanning speed and hatching spacing) are specified on each test matrix.

Even if these manufacturing conditions cannot be considered optimal, a power of 54W, a scanning speed of 100 mm.s^{-1} and a hatch spacing of 20 micrometers, were finally chosen to manufacture the metallic areas of the multi-material parts, which will be presented at the end of the article. The material obtained is an aluminum-silicon metal alloy, which however contains alpha alumina as well as very low contents of the allotropic varieties β, δ and γ of this oxide (Fig. 11). The metal alloy is less rich in aluminum than the starting AlSi12 powder, given the partial oxidation of the aluminum. The relative intensities of the peaks of silicon, compared to those of aluminum, are in fact greater for the alloy obtained by laser melting than for the initial AlSi12 powder. Despite the presence of a small amount of oxide, the alloy resulting from the additive manufacturing has an electrical conductivity of the metallic type.

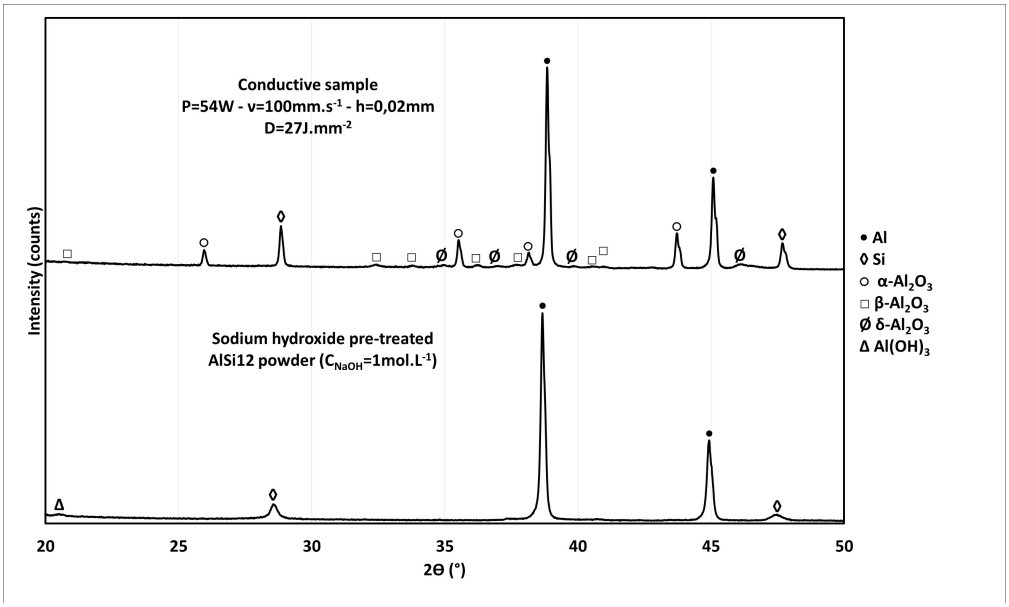

Figure 11 : X-ray diffraction patterns of sodium hydroxide pre-treated AlSi12 powder with 1mol.L^{-1} concentrated solution and bulk conductive sample obtained after laser powder bed fusion.

3.4. Dielectric ceramic areas

Obtaining ceramic areas is more challenging because it requires both oxidation and sintering of an alumina-type refractory material. The simplified equation [27] describing the evolution of the oxidized thickness over time on the surface of a metal, teaches that oxidized part of a metal increases with oxygen partial pressure, temperature and time:

$$X \propto t^{0.5} . e^{-Q/RT} . (P_{O2})^{1/n} \quad (7)$$

with:

X: thickness of the oxidized layer
t : oxidation time
Q: Energy of activation
T: temperature
P_{O2} : oxygen partial pressure
n: constant.

The partial pressure of oxygen being fixed by the air contained in the chamber of the machine, the question is how the temperature and the time can be influenced by the choice of the manufacturing parameters.

The thermal effects created on the surface unit of the powder bed depend on the energy provided by the laser spot. The more this energy increases, the higher the temperature at the surface of the powder. For a unit area of a powder bed, the laser heating time "t" is such that:

$$t = 1 / (v.h). \quad (8),$$

h is the hatch spacing,
v is the scanning speed of the laser spot.

The energy per unit surface area "E" (energy density) received, will be therefore :

$$E = P / (v.h) \quad (9),$$

P is the laser power.

Even if the energy density area provided (P / (v.h)) will be significantly consumed by radiation and thermal conduction in particular, it will be the basis of the temperature rise responsible for the physicochemical transformations (melting, oxidation, sintering, etc…) undergone by the powder bed. Furthermore, the time during which the powder bed will be maintained at a high temperature, allowing in particular the progression of the oxidation, will increase as a function of $(1/(v.h))^{0,5}$. For all of these reasons, it appears that the manufacturing parameters h, v and P are very important and that the most favorable conditions for obtaining an oxide-type material will be sought for combinations giving mainly high E = P / (v.h) values.

The exploration of the manufacturing conditions was however limited by the minimum power necessary to obtain sintered parts (P ≥ 35 W) and the maximum power allowing to avoid the powder expulsion (P ≤ 90 W). Although paying great attention to the low values of h and v, the ranges tested were 1 to 16 μm and 100 to 1600 $mm.s^{-1}$. It was thus possible to have samples that differ greatly in the energy E received per unit area. The samples produced at the highest energy densities are represented by circles on the graph showing the laser power used, as a function of the product of the parameters h and v (Fig. 12). On this graph, the line P = E.(v.h) with E= 36 $J.mm^{-2}$, is also plotted. The figure 12 thus shows a phase diagram in which are grouped together in the zones where the energy densities E are the highest (empty circles), the dielectric samples consisting mainly of aluminum oxides. The conductive samples, which are essentially metallic in nature, are for their part, located in the areas for which E is lower (solid circles). The energy per unit area defining the boundary between these two regions is indicated by a dotted line. It is close to 36 $J.mm^{-2}$. The horizontal dotted lines define approximately the regions for obtaining coherent parts.

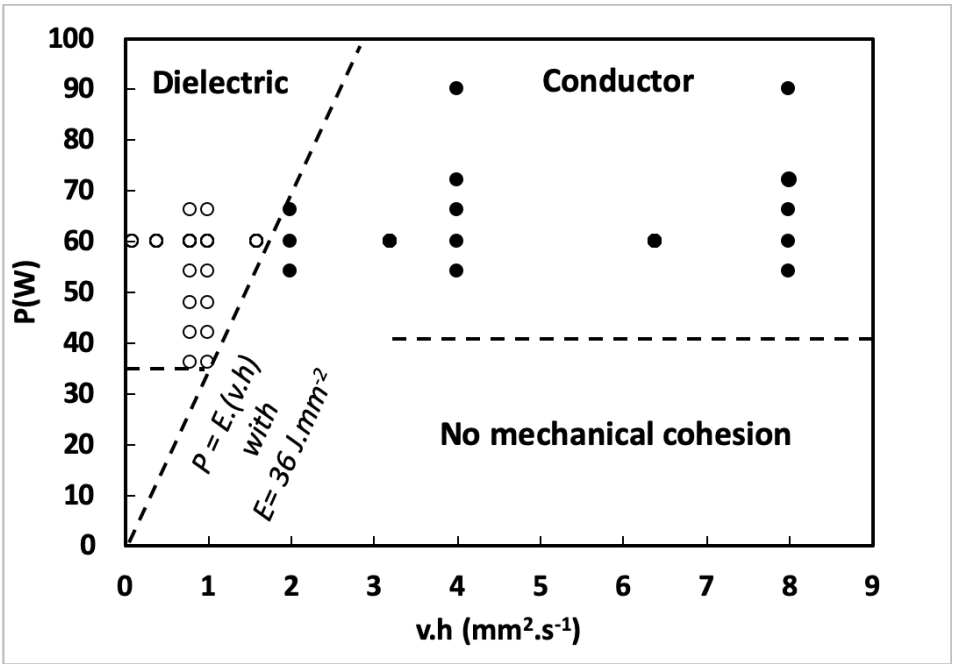

Figure 12 : Phase diagram of samples obtained for different values of laser power P and different product of hatch spacing h and laser scanning speed v.

Three characteristic insulating samples, obtained under conditions of identical scanning speed and hatch spacing (1000 $mm.s^{-1}$ and 1 μm) but at different powers (36, 54 and 66 W), show mainly the α-Al_2O_3 phase in their X-ray diffractogram (Fig. 13). This is however accompanied by a residue of metallic silicon and even of aluminum, for the sample obtained at the lowest power and whose value of E calculated according to equation (9), is close to the limit separating the conductive and insulating materials in figure 12. We also note the presence of additional diffraction peaks attributed to the δ-$Al_{196}O_{288}N_4$ and γ-$Al_{28}1O_{356}N_4$ varieties of aluminum oxynitrides. According to Corbin [28], these phases could form by reaction between liquid aluminum and air around 1500 °C. It is therefore not surprising to detect their presence in samples obtained by laser fusion, since it has already been shown that such temperatures are exceeded during the additive manufacturing of ceramic-metal

composites [29] or laser decomposition of metal organic compounds [30][31]. A very low intensity peak also suggests the existence of traces of aluminum nitride. All these phases are revealed on the surface of the samples, but also within their cross section, with the exception of metallic aluminum, which could only be detected on the surface of one sample only.

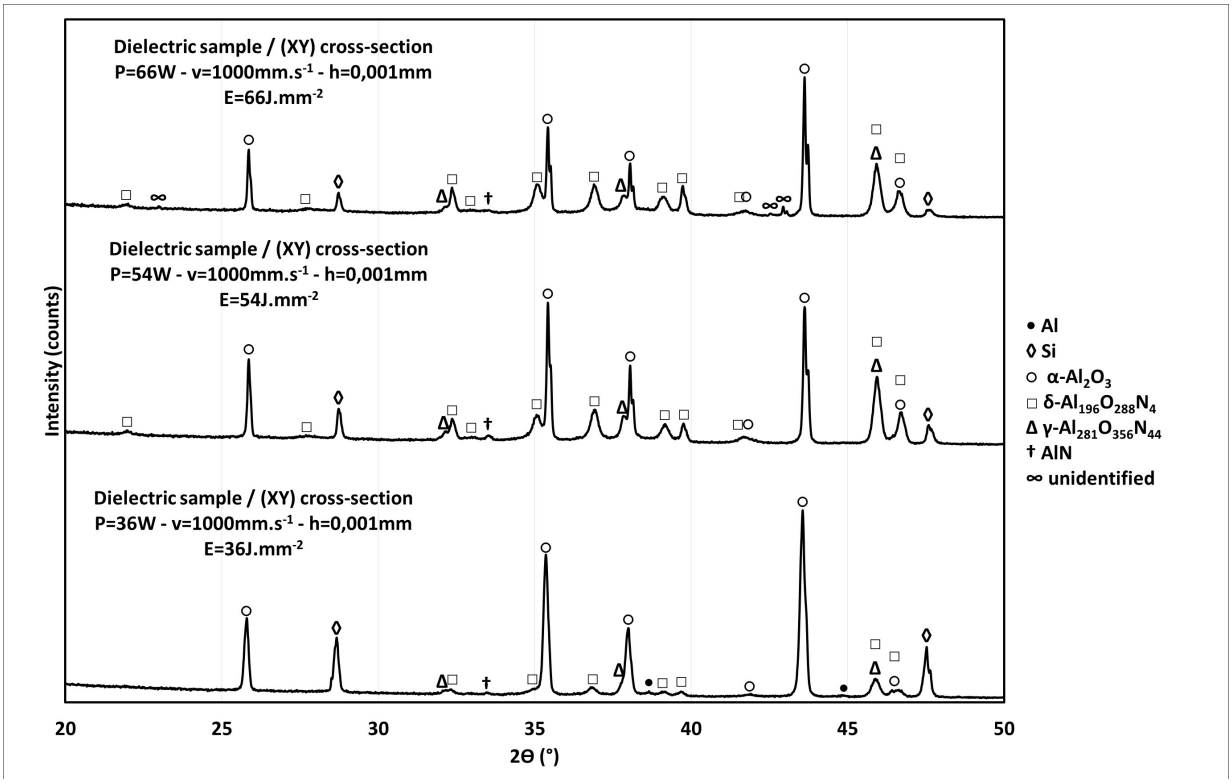

Figure 13 : X-Ray diffractograms of dielectric sample cross-sections (XY plane) obtained by selective oxidation of sodium hydroxide pre-treated AlSi12 powder (C_{NaOH}=1mol.L^{-1}) under air. Different specific laser beam parameters (different energies per surface unit) were implemented.

Infrared spectroscopy (Fig. 14) shows bands characteristic of alpha alumina thus confirming the previous results. This technique also shows a broad band of low intensity, which testify to the presence of Si-O bonds in sodium aluminosilicate $NaAlSiO_4$, identified in the powders treated with sodium hydroxide. This compound is detected primarily for the sample prepared under high laser power (66 W).

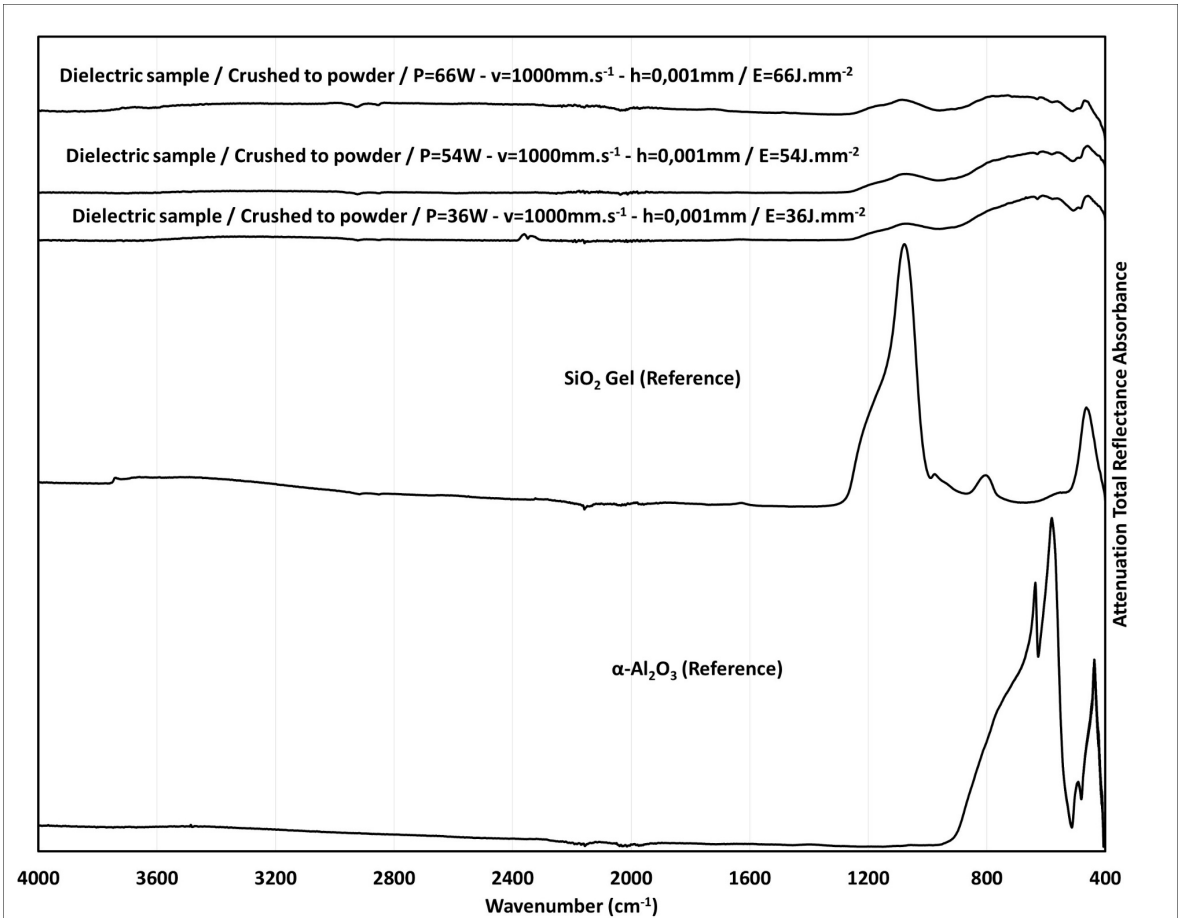

Figure 14: Infrared spectra of crushed to powder dielectric samples obtained by selective oxidation of sodium hydroxide pre-treated AlSi12 powder (C_{NaOH}=1mol.L^{-1}) under air atmosphere with specific laser beam parameters (different energies per surface unit) and material references.

The samples studied above are relatively rough (Ra close to 130 μm). Observation of transverse sections also reveals a microstructure in regular strata of about 250 μm thick (Fig. 15). This value is approximately five times greater than the 50 μm thickness of the powder beds, successively spread during the manufacture of the parts. Stratification is therefore not directly related to the adjustment of the powder supply to the part construction area. EDS analyses show that the strata are essentially made up of aluminum and oxygen, in good agreement with the predominance of alumina in the samples previously studied by X-ray diffraction. The areas separating two successive strata, however concentrate the elements sodium and silicon. The latter is more in the metallic state, the electron micrograph indeed showing a strong contrast of these regions. Sodium is very probably involved in the aluminosilicate previously identified by infrared spectroscopy. The concentration of metallic silicon and sodium aluminosilicate, could result from their diffusion on the surface of the layers melted by the laser. Their accumulation as the part is built, especially after stacking about five layers, would allow them to reach a critical proportion causing dissociation with the part containing predominantly alumina. This is how cracks would form and a relatively large porosity would develop between two strata, near the areas mainly containing metallic silicon and sodium aluminosilicate. This interpretation must be subsequently confirmed by varying, in particular, the silicon and sodium contents of the powder, used by the manufacturing process.

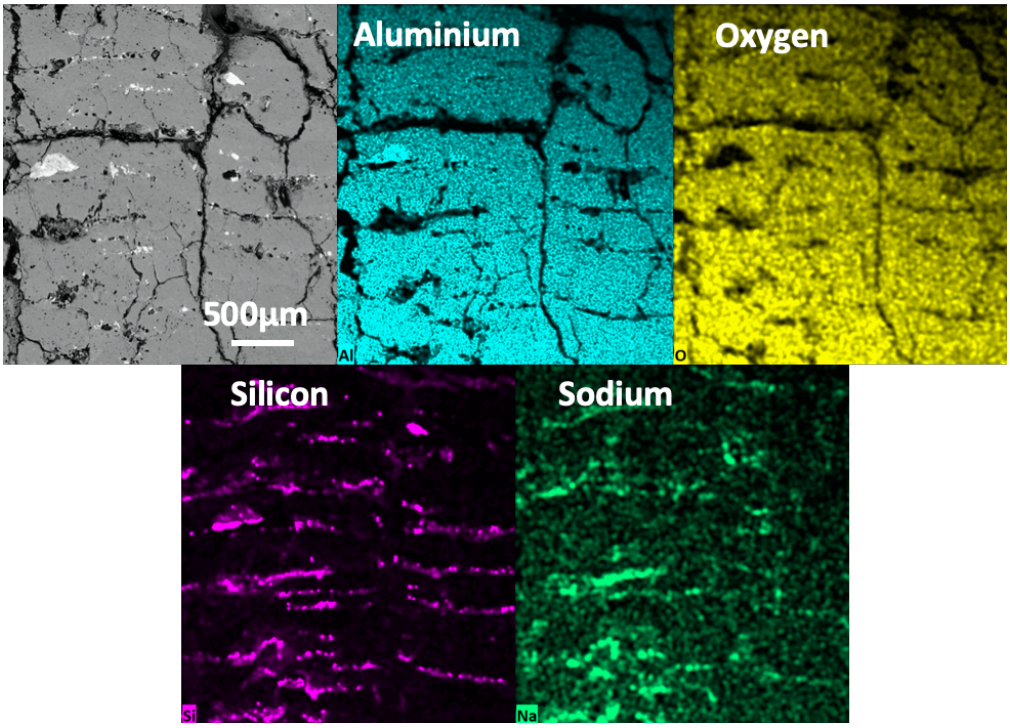

Figure 15 : Cross-section view of a ceramic obtained at P = 60 W, v = 800 mm.s-1 and h = 0.001 mm with related EDX chemical maps.

The density of the ceramic cubes produced was measured from their mass and volume. The values obtained for the power range examined are compiled in Table 1. The highest densities (2.8 g.cm^{-3}) are obtained for the highest powers used. They correspond to a relative density of about 70%, if we consider that the material resulting from the oxidation consists of 100% alumina.

Dielectric samples obtained by selective laser beam oxidation	Measured density (g.cm^{-3})	Relative density considering samples are pure α-Al_2O_3
P=36W – v=1000mm.s^{-1} – h=0,001mm D=36J.mm^{-2}	2,08	52%
P=42W – v=1000mm.s^{-1} – h=0,001mm D=42J.mm^{-2}	1,79	45%
P=48W – v=1000mm.s^{-1} – h=0,001mm D=48J.mm^{-2}	2,71	68%
P=54W – v=1000mm.s^{-1} – h=0,001mm D=54J.mm^{-2}	2,63	66%
P=60W – v=1000mm.s^{-1} – h=0,001mm D=60J.mm^{-2}	2,79	70%
P=66W – v=1000mm.s^{-1} – h=0,001mm D=66J.mm^{-2}	2,80	70%

Table 1: Densities and relative densities of dielectric samples manufactured with specific laser beam parameters (energy per unit surface).

Relative permittivity of some ceramic samples, manufactured with different laser parameters, have been identified by means of microwave network analyzer (Table 2). For the greatest energies per surface unit, relative permittivity of ceramic samples is close to α alumina [32] and silicon [33] relative permittivity.

Sample	Energy density E ($J.mm^{-2}$)	Relative permittivity (1 to 20GHz)
Cylinder (Ø=30mm, H=10mm)	63	8 – 5
Plate (50 x 50 x 2 mm^3)	67	8.5 – 5
Plate (20 x 20 x 2 mm^3)	67	10 – 6.5
Plate (20 x 20 x 2 mm^3)	74	11 – 8

Table 2: Relative permittivity of ceramic samples with different dimensions and manufactured with different surface energy densities

3.5. Multi-materials parts with metallic and dielectric areas

The conditions for the development of metallic or dielectric areas having been identified, the production of multi-material parts from a single powder became possible. A few parts intended to demonstrate the feasibility, were therefore produced using the manufacturing conditions reported in Table 2.

Conductive areas	Dielectric areas
P=60W – v=100mm.s^{-1} – h=0,05mm E = 12 $J.mm^{-2}$	P=60W – v=1000mm.s^{-1} – h=0,001mm E = 60 $J.mm^{-2}$

Tableau 2 : Manufacturing conditions for multi-material parts.

The assemblies obtained (Fig. 16) show the association of the dielectric parts of gray color with the predominantly metallic parts of black color. The dielectric ceramic areas are not completely white as one would expect from a material consisting essentially of alumina. However, no heterogeneity of composition was observed at the surface of the samples. Taking into account the observations of cross sections, which reveal strata containing metallic silicon, it is possible that the shades of gray observed result from these regions concentrating small quantities of metal. These regions could thus be perceived by transparency. It has also been observed that the side faces of the ceramic parts are not very well defined when they are not in contact with a merged metal wall. The formation of the ceramic therefore takes place in a better controlled geometry when it is confined in even relatively thin metal walls (about 0.5 mm).

Figure 16 : 3D multi-material parts composed of conductive areas (black) and dielectric areas (grey)(side of multi-material squares: 2 cm).

The ceramic-metal interface is not perfectly smooth (Fig. 17). In fact, an interpenetration of the oxide phases and of the metal, is observed over a thickness of approximately 200 micrometers. For the manufacturing of certain microwave devices, this interface will have to be improved in the future. As the entire area where the dielectric materials are located in the diagram of figure 13, has not yet been explored, it seems possible to improve the ceramic-metal interfaces. In addition, specific part construction strategies can be considered on either side of the interfaces, to achieve better ceramic-metal assemblies. There are therefore real prospects for improvement.

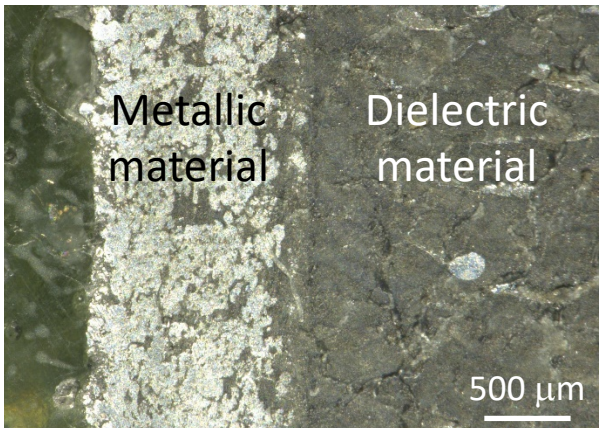

Figure 17 : Interface between dielectric ceramic and metallic region in a multi-material part fabricated by laser fusion on powder bed.

4. Conclusion

The feasibility of manufacturing by laser fusion on a powder bed, multi-material parts made up in the three directions of the space, of ceramic or metal zones, was demonstrated during this work. Such parts could be of interest for instance, to microwave electronics since they can potentially associate, in complex geometries, an electrically conductive metal with an insulating ceramic material of high dielectric constant.

The process developed uses a single AlSi12 alloy powder previously activated with a sodium hydroxide solution. This treatment allows the compact and protective passivation layer of the starting alloy to be replaced by a more porous layer. The powder thus activated then becomes easier to oxidize and it is then possible to manufacture multi-material parts from a single powder. To achieve the production of multi-material parts, it is however necessary to apply differentiated manufacturing conditions depending on whether one wishes to obtain a metallic or ceramic zone. It is shown that obtaining and sintering oxides requires adjusting the manufacturing parameters so that the laser provides an energy per unit area E, which is higher than for the melting in the metallic state of the activated powder. The manufacturing parameters to be set as a priority are the power P of the laser beam, its scanning speed v and the hatch spacing h. The energy E supplied per unit area of the powder bed using the laser, is in fact equal to the ratio P /(v.h). When E is less than approximately 36 $J.mm^{-2}$, the material obtained is predominantly metallic. It then conducts electricity. For higher E values, a ceramic predominantly made up of alumina, is formed and sintered. The material obtained is then dielectric (dielectric constant # 8).

The three-dimensional ceramic-metal associations obtained by laser fusion still suffer from some imperfections. The surface of the parts is relatively rough, especially in the ceramic regions, which are otherwise modestly densified (less than 70%). The ceramic-to-metal interfaces are also quite rough. All of these characteristics will therefore have to be improved in the future with a view to producing devices for the space industry or other sectors of activity wishing to combine in complex geometries, a ceramic and a metal. However, different degrees of freedom not yet exploited, point to future positive developments.

References

[1] ISO/ASTM 52900:2015 - Additive manufacturing - General principles - Terminology, (2015).

[2] M. Jiménez, L. Romero, I.A. Domínguez, M.D.M. Espinosa, M. Domínguez, Additive Manufacturing Technologies: An Overview about 3D Printing Methods and Future Prospects, Complexity. 2019 (2019). https://doi.org/10.1155/2019/9656938.

[3] R. Paknys, Waveguides and Resonators, in: Appl. Freq. Electromagn., First Edit, Wiley-IEEE Press, 2016: pp. 69–128. https://doi.org/10.1002/9781119127444.ch3.

[4] S. Lathabai, Additive Manufacturing of Aluminium-Based Alloys and Composites, Elsevier Ltd., 2018. https://doi.org/10.1016/b978-0-08-102063-0.00002-3.

[5] N.T. Aboulkhair, M. Simonelli, L. Parry, I. Ashcroft, C. Tuck, R. Hague, 3D printing of Aluminium alloys: Additive Manufacturing of Aluminium alloys using selective laser melting, Prog. Mater. Sci. 106 (2019) 100578. https://doi.org/10.1016/j.pmatsci.2019.100578.

[6] P. Ponnusamy, R.A.R. Rashid, S.H. Masood, D. Ruan, S. Palanisamy, Mechanical properties of slm-printed aluminium alloys: A review, Materials (Basel). 13 (2020) 1–51. https://doi.org/10.3390/ma13194301.

[7] P. Vora, K. Mumtaz, I. Todd, N. Hopkinson, AlSi12 in-situ alloy formation and residual stress reduction using anchorless selective laser melting, Addit. Manuf. 7 (2015) 12–19. https://doi.org/10.1016/j.addma.2015.06.003.

[8] C. Vargel, Aluminium casting alloys, in: Corros. Alum., 2e ed., Elsevier, 2020: pp. 525–537. https://doi.org/10.1016/b978-0-08-099925-8.00038-7.
[9] P.A. Lykov, R.M. Baitimerov, Selective laser melting of alsi12 powder, Solid State Phenom. 284 SSP (2018) 667–672. https://doi.org/10.4028/www.scientific.net/SSP.284.667.
[10] S. Siddique, M. Imran, E. Wycisk, C. Emmelmann, F. Walther, Fatigue Assessment of Laser Additive Manufactured AlSi12 Eutectic Alloy in the Very High Cycle Fatigue (VHCF) Range up to 1E9 cycles, Mater. Today Proc. 3 (2016) 2853–2860. https://doi.org/10.1016/j.matpr.2016.07.004.
[11] Senvol, (2021). http://senvol.com/ (accessed March 5, 2021).
[12] J. Zhao, M. Easton, M. Qian, M. Leary, M. Brandt, Effect of building direction on porosity and fatigue life of selective laser melted AlSi12Mg alloy, Mater. Sci. Eng. A. 729 (2018) 76–85. https://doi.org/10.1016/j.msea.2018.05.040.
[13] D.J. Young, Enabling Theory, in: High Temp. Oxid. Corros. Met., 2016: pp. 31–84. https://doi.org/10.1016/b978-0-08-100101-1.00002-9.
[14] Y. Chen, D.R. Guildenbecher, K.N.G. Hoffmeister, M.A. Cooper, H.L. Stauffacher, M.S. Oliver, E.B. Washburn, Study of aluminum particle combustion in solid propellant plumes using digital in-line holography and imaging pyrometry, Combust. Flame. 182 (2017) 225–237. https://doi.org/10.1016/j.combustflame.2017.04.016.
[15] Z. Hu, T. Yang, Z. Xia, L. Ma, M. Li, Y. Feng, The Simulation of Different Combustion Stages of Micron-Sized Aluminum Particles, Appl. Sci. (2021) 1–16. https://doi.org/10.3390/app11041774.
[16] C. Rossi, K. Zhang, D. Estève, P. Alphonse, P. Tailhades, C. Vahlas, Nanoenergetic materials for MEMS: A review, J. Microelectromechanical Syst. 16 (2007) 919–931. https://doi.org/10.1109/JMEMS.2007.893519.
[17] M.A. Trunov, M. Schoenitz, X. Zhu, E.L. Dreizin, Effect of polymorphic phase transformations in Al2O3 film on oxidation kinetics of aluminum powders, Combust. Flame. 140 (2005) 310–318. https://doi.org/10.1016/j.combustflame.2004.10.010.
[18] L. Kovarik, M. Bowden, J. Szanyi, High temperature transition aluminas in δ-Al2O3/θ-Al2O3 stability range: Review, J. Catal. 393 (2021) 357–368. https://doi.org/10.1016/j.jcat.2020.10.009.
[19] S. Mirhashemihaghighi, J. Światowska, V. Maurice, A. Seyeux, S. Zanna, E. Salmi, M. Ritala, P. Marcus, Corrosion protection of aluminium by ultra-thin atomic layer deposited alumina coatings, Corros. Sci. 106 (2016) 16–24. https://doi.org/10.1016/j.corsci.2016.01.021.
[20] Z. Ahmad, Atmospheric Corrosion, in: Princ. Corros. Eng. Corros. Control, 2006: pp. 550–575. https://doi.org/10.1016/B978-075065924-6/50011-8.
[21] J. Joys, Production of Aluminum and Aluminum-Alloy Powder, in: Powder Metall., ASM International, 2015. https://doi.org/10.31399/asm.hb.v07.9781627081757.
[22] C. Vargel, Inorganic bases, in: Corros. Alum., Elsevier Ltd, 2020: pp. 659–665. https://doi.org/10.1016/B978-0-08-099925-8.00051-X.
[23] C. Vargel, Inorganic acids, in: Corros. Alum., Elsevier Ltd, 2020: pp. 667–681. https://doi.org/10.1016/b978-0-08-099925-8.00052-1.
[24] P. Godart, J. Fischman, K. Seto, D. Hart, Hydrogen production from aluminum-water reactions subject to varied pressures and temperatures, Int. J. Hydrogen Energy. 44 (2019) 11448–11458. https://doi.org/10.1016/j.ijhydene.2019.03.140.
[25] S. Shayanfar, V. Aghazadeh, A. Saravari, P. Hasanpour, Aluminum hydroxide

crystallization from aluminate solution using carbon dioxide gas : Effect of temperature and time, J. Cryst. Growth. 496–497 (2018) 1–9. https://doi.org/10.1016/j.jcrysgro.2018.04.028.
[26] A. Bolt, I. Dincer, M. Agelin-Chaab, Experimental study of hydrogen production process with aluminum and water, Int. J. Hydrogen Energy. 45 (2020) 14232–14244. https://doi.org/10.1016/j.ijhydene.2020.03.160.
[27] D.J. Young, Oxidation of Pure Metals, in: High Temp. Oxid. Corros. Met., Elsevier Ltd, 2016: pp. 85–144. https://doi.org/10.1016/b978-0-08-100101-1.00003-0.
[28] N.D. Corbin, Aluminum oxynitride spinel: A review, J. Eur. Ceram. Soc. 5 (1989) 143–154. https://doi.org/10.1016/0955-2219(89)90030-7.
[29] I. Pasquet, V. Baco-Carles, P. Chamelot, M. Gibilaro, L. Massot, P. Tailhades, A multi-material based on metallic copper and spinel oxide made by powder bed laser fusion: A new nanostructured material for inert anode dedicated to aluminum electrolysis, J. Mater. Process. Technol. 278 (2020) 116452. https://doi.org/10.1016/j.jmatprotec.2019.116452.
[30] I. Pasquet, H. Le Trong, V. Baco-Carles, L. Presmanes, C. Bonningue, V. Baylac, P. Tailhades, V. Conedera, P.F. Calmon, D. Dragomirescu, H. Camon, Direct shaping of oxides by laser insolation of transition metal oxalates, J. Eur. Ceram. Soc. 37 (2017) 5315–5320. https://doi.org/10.1016/j.jeurceramsoc.2017.03.030.
[31] I. Pasquet, H. Le Trong, V. Baco, V. Conédéra, H. Camon, P. Tailhades, Selective Laser Decomposition of Silver Oxalate: A New Way of Preparing and Shaping Metallic Silver Patterns, Lasers Manuf. Mater. Process. 7 (2020) 513–531. https://doi.org/10.1007/s40516-020-00131-1.
[32] M.T. Sebastian, Alumina, Titania, Ceria, Silicate, Tungstate and Other Materials, in: Dielectr. Mater. Wirel. Commun., Elsevier Ltd, 2008: pp. 379–443. https://doi.org/10.1016/b978-0-08-045330-9.00011-x.
[33] M.T. Sebastian, List of Microwave Dielectric Resonator Materials and their Properties, in: Dielectr. Mater. Wirel. Commun., Elsevier Ltd, 2008: pp. 541–652. https://doi.org/10.1016/B978-0-08-045330-9.00018-2.

Acknowledgements : This work benefited from the help of the MultiFab platform funded by the Occitanie Region and the European Regional Development Fund. The authors thank Vincent Baylac and Matthieu Bugeau for their technical support.